Supplementary Material

Station name	Latitude (°N)	Longitude (°E)	Elevation (m)
CORR	44.90190	11.00944	20
ROCC	44.90000	10.92417	17
ROVE	44.85307	10.94972	21
SGIA	44.85917	11.03583	20

Table S1. List of the four local network VO stations: names, coordinates in degrees, and elevation in m from sea level.

Station name	Latitude (°N)	Longitude (°E)	Elevation (m)
CAVE	44.86580	11.00310	18
FERS	44.90350	11.54060	3
FIU	44.64031	11.49165	12
MNTV	45.14950	10.78970	36
MODE	44.62972	10.94917	41
NDIM	44.88730	10.89870	19
OPPE	45.30820	11.17240	20
RAVA	44.75587	11.11880	15
SBPO	45.05108	10.91987	10
SERM	45.00997	11.29582	7

Table S2. List of the ten Italian Seismic Network IV stations: names, coordinates in degrees, and elevation in m from sea level.

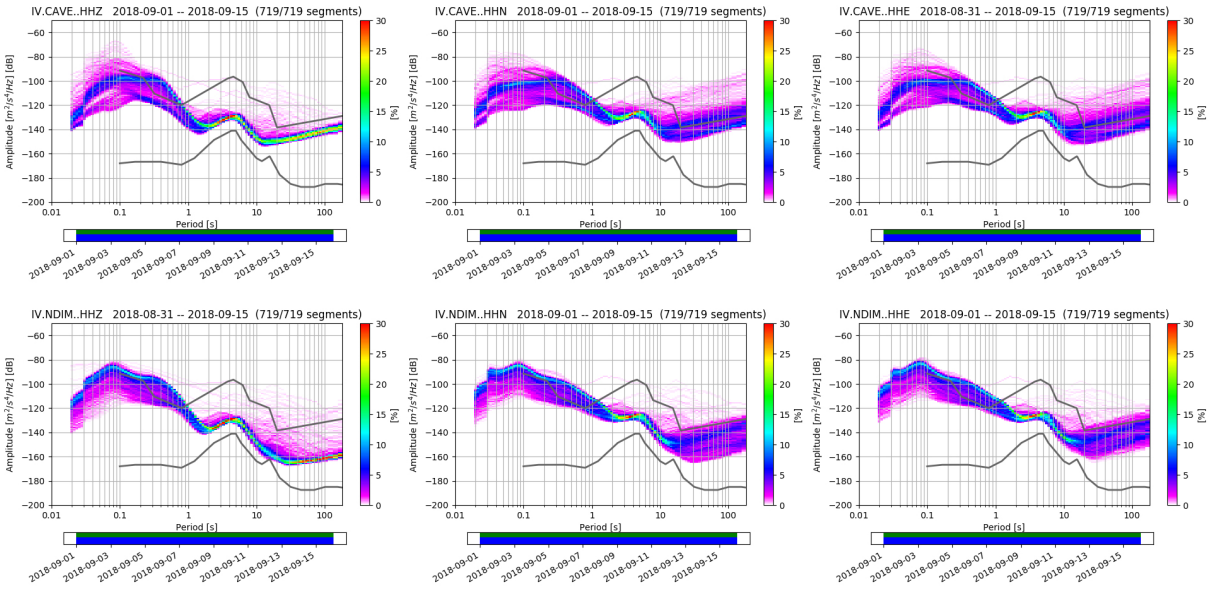

Figure S1. Power Spectral Densities for the 2 IV stations CAVE and NDIM at their 3 components. Each row correspond to a station (in alphabetical order from top to bottom): CORR, ROCC, ROVE, SGIA; and each column to a component: EHZ, EHN, EHE (from left to right). The black lines highlight the NHNM and NLMN curves defined by Peterson (1993). The blue/green bar on the bottom shows the data under analysis (blue), and the data availability (in green), at that particular station/channel, they are coincident since we took all available data in this case.

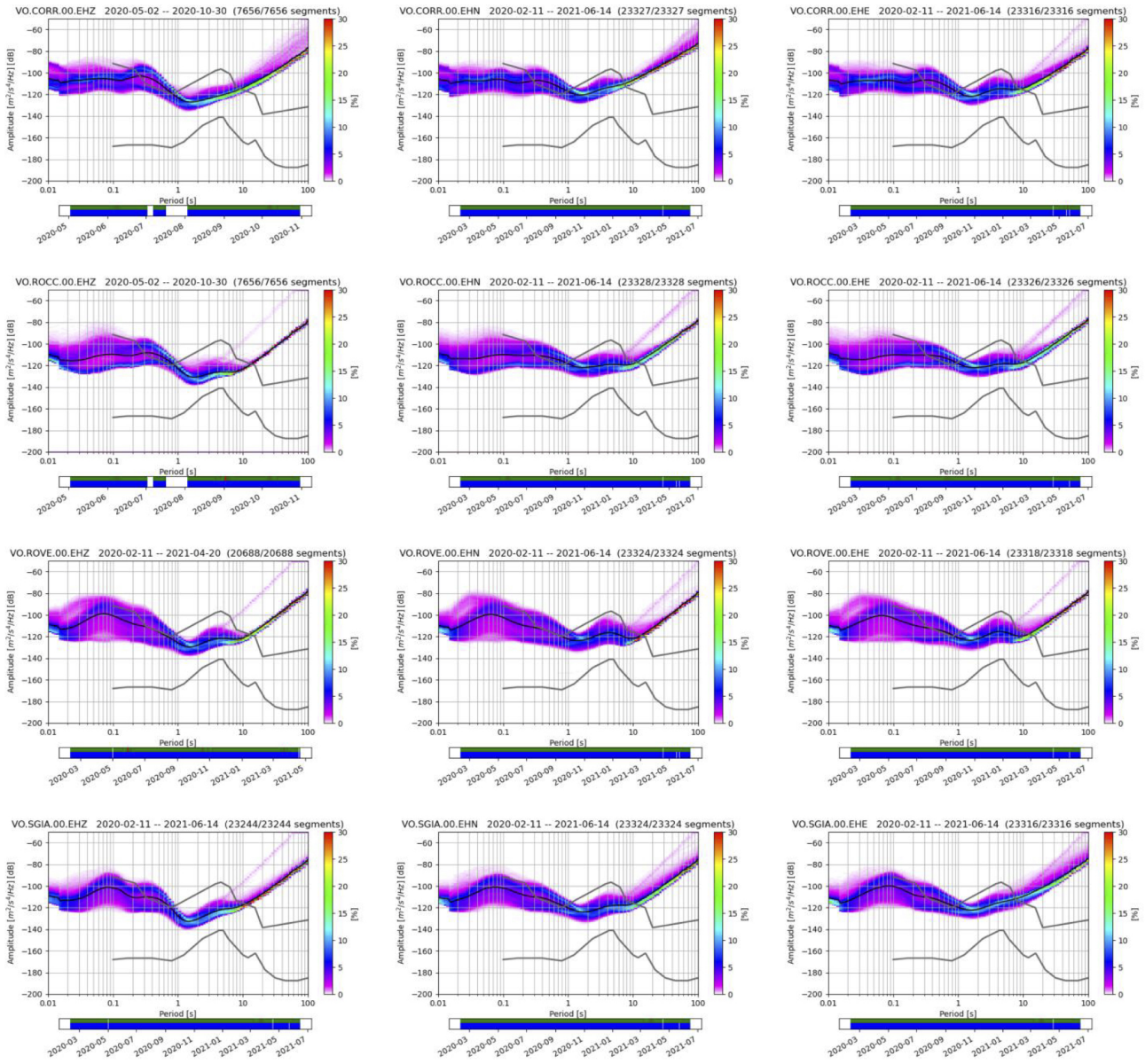

Figure S2. Power Spectral Densities for the 4 VO stations at their 3 components, obtained from the continuous data we could profit after the local network improvement operated on December 2018. Each row correspond to a station (in alphabetical order from top to bottom): CORR, ROCC, ROVE, SGIA; and each column to a component: EHZ, EHN, EHE (from left to right). The black lines highlight the NHNM and NLNM curves defined by Peterson (1993). The blue/green bar on the bottom shows the data under analysis (blue), and the data availability (in green), at that particular station/channel, they are coincident since we took all available data in this case.

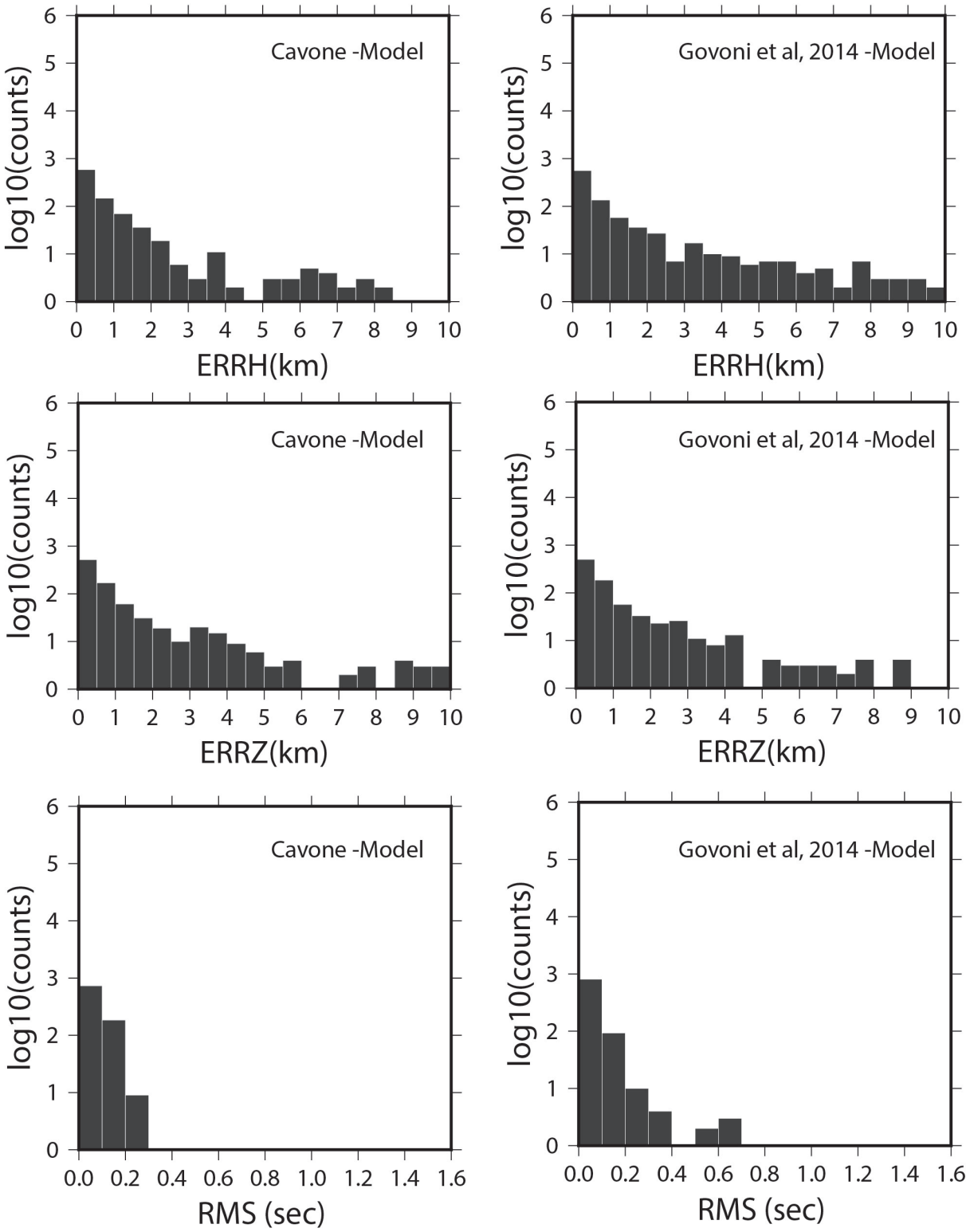

Figure S3. The histograms report the measurement errors associated to the location of thousands of seismic events detected during the 2012 Emilia sequence. From top to bottom we show the comparison of horizontal and vertical errors, and RMS values, respectively, obtained for the two velocity models available for this area. On the left column the "Cavone-Model" , the local velocity model created ad-hoc for the Cavone oil field owned by the operator (reported in the Supplementary Table 3). On the right column the Govoni et al. (2014) one generated on the basis of the 2012 Emilia earthquake sequence ("Govoni et al 2014-Model").

v_P **(km/s)**	**Depth (km)**	v_P/v_S
1.7	0	1.73
2.1	0.2	1.73
2.7	1.5	1.73
5.0	5.5	1.73
6.3	11	1.73
8.2	24	1.73

Table S3. Velocity model for the Cavone oil field as provided by the operator (Società Padana Energia, personal communication, 2018).

N	Date	Longitude	Latitude	Depth	errH	errZ	RMS	GAP	Picks
	yyyy-mo-dd hh:mi	°E	°N	km	km	km	s	deg	
1	2018-03-03 20:12	11.1507	44.8317	7.82	0.3	0.5	0.23	252	12
2	2018-03-04 14:37	11.0108	44.8870	5.68	0.1	0.1	0.07	151	10
3	2018-03-07 15:10	11.1447	44.8448	6.86	0.3	1.0	0.13	251	10
4	2018-05-27 03:31	10.9633	44.8867	5.11	0.1	0.2	0.13	129	13
5	2018-08-03 21:14	10.9485	44.8915	5.44	0.3	0.2	0.08	140	13
6	2018-08-05 04:07	10.9523	44.8928	4.11	0.2	0.4	0.16	148	12
7	2018-08-27 04:08	10.9972	44.8845	5.93	0.3	0.4	0.06	112	9
8	2018-09-12 13:29	10.9740	44.8902	4.70	0.3	0.2	0.07	200	8
9	2018-09-15 20:00	10.9847	44.8918	5.54	0.4	n.d.	0.05	211	6
10	2018-10-23 14:11	11.0147	44.8825	4.46	0.4	0.4	0.11	230	8
11	2018-11-24 02:04	10.9242	44.8932	5.47	0.4	0.2	0.05	104	12
12	2018-11-25 23:32	11.0232	44.8327	10.35	0.5	0.6	0.01	273	7
13	2018-12-11 19:24	11.0733	44.8943	6.98	0.7	0.7	0.14	247	10
14	2019-01-10 23:53	10.9607	44.8927	0.27	0.2	n.d.	1.13	169	7
15	2019-01-17 01:03	10.9275	44.8865	6.89	0.6	0.8	0.07	125	8
16	2019-01-19 10:16	11.0187	44,9605	1.79	1.1	n.d.	4.13	316	9
17	2019-03-03 15:21	11.0512	44.8780	5.39	1.3	0.2	0.03	313	6
18	2019-03-03 16:08	11.0398	44.8560	5.30	0.5	0.1	0.08	292	8
19	2019-03-07 02:30	11.0327	44.8617	5.94	0.5	0.5	0.15	160	11
20	2019-03-13 14:22	11.2145	44.8447	18.21	2.4	2.4	0.18	286	14
21	2019-03-23 03:53	10.9770	44.8807	5.88	1.2	1.4	0.04	262	6
22	2019-03-27 16:36	10.5940	44.8362	20.25	7.0	8.2	0.32	350	6
23	2019-05-04 23:01	11.2380	44.8582	17.10	0.7	1.6	0.21	205	11
24	2019-05-12 15:24	11.1037	44.8957	10.75	1.0	0.9	0.13	318	8
25	2019-05-28 20:07	11.0153	44.8805	5.73	0.7	0.4	0.03	237	6
26	2019-06-16 10:49	10.9988	44.8593	7.11	0.3	0.5	0.06	170	9
27	2019-06-18 00:57	11.0137	44.8582	7.65	0.3	0.5	0.10	177	11
28	2019-06-18 22:26	11.0202	44.8763	5.68	0.2	0.3	0.05	164	11
29	2019-06-30 17:49	11.0242	44.8768	5.42	0.3	0.1	0.16	173	13
30	2019-06-30 22:59	11.0233	44.8752	5.26	0.2	0.1	0.10	170	14
31	2019-07-13 04:18	10.9245	44.8928	5.41	0.3	0.1	0.06	105	10
32	2019-07-15 05:48	10.8757	44.8688	9.12	0.5	0.6	0.21	301	10
33	2019-07-18 00:13	10.6917	44.8217	11.11	1.7	n.d.	0.23	343	11
34	2019-07-20 21:08	10.9245	44.8928	5.43	0.2	0.1	0.06	117	8
35	2019-07-27 11:11	10.9398	44.8895	6.31	0.1	0.4	0.08	123	13
36	2019-07-27 11:12	10.9437	44.8950	6.45	0.2	0.4	0.09	151	10
37	2019-07-31 22:49	11.0233	44.8197	8.63	0.3	0.6	0.14	169	14
38	2019-08-18 20:23	10.9723	44.8917	5.58	0.4	1.4	0.07	145	11
39	2019-08-26 04:02	10.8762	44.8667	8.98	0.6	0.6	0.06	291	7
40	2019-09-03 00:48	11.0017	44.8730	5.81	0.2	0.2	0.04	129	8
41	2019-09-03 02:49	11.0177	44.8710	6.13	0.3	0.4	0.06	143	10
42	2019-09-18 19:59	10.9062	44.8888	8.77	n.d.	n.d.	0.01	180	4
43	2019-09-18 20:00	10.9042	44.8892	8.91	n.d.	n.d.	0.01	180	4
44	2019-10-01 21:29	11.030	44.8767	5.39	0.4	0.1	0.05	196	8
45	2019-10-04 13:23	11.3345	44.8995	11.21	0.7	n.d.	0.21	137	12
46	2019-10-31 08:22	11.0410	44.9650	13.89	5.4	6.7	0.49	324	7
47	2019-11-25 00:03	10.9127	44.8883	5.60	0.6	1.0	0.08	138	8
48	2019-12-03 08:42	10.9218	44.9023	6.91	0.8	0.9	0.16	219	9
49	2019-12-18 18:07	11.2583	44.8502	11.36	1.2	n.d.	0.71	217	5

Table S4. List of the 49 earthquakes analysed during 2018-2019. The date is expressed in year-month-day, then we report location estimates (longitude, latitude and depths in km), horizontal and vertical errors on the location in km (errH and errZ respectively), RMS in seconds, azimuthal gap of the station used for locating the event, and number of picks used for location. We can observe that the events with less detected phase arrivals show the bigger errors in locations or even a not defined value ("n.d.").

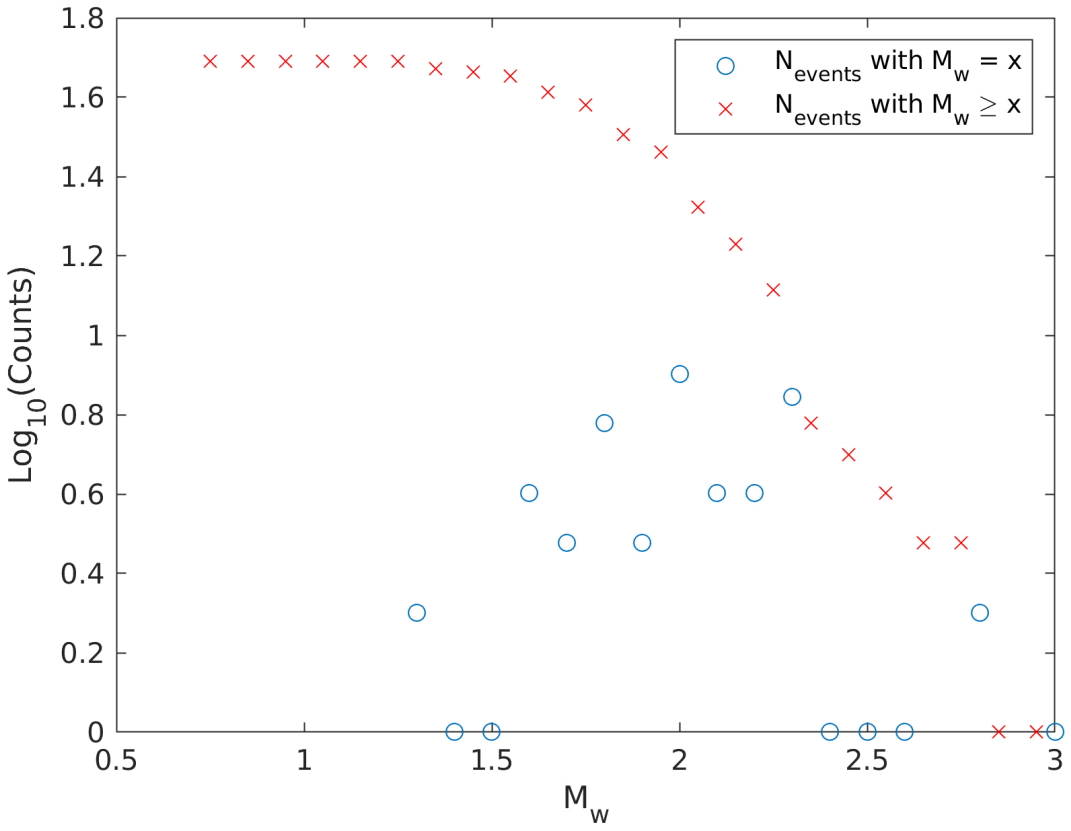

Figure S4. Logarithm of the event counted per moment magnitude M_W, the blue circles indicate all events with magnitude equal to M_W while the red crosses the number of events with magnitude equal or greater than M_W (the cumulated number of events). We test the stability of the completeness magnitude by performing the computation through three different methodologies: Marzocchi et al. (2016); Wiemer and Wyss (2000); Woessner and Wiemer (2005), and we obtain the same value of $Mc = 2$

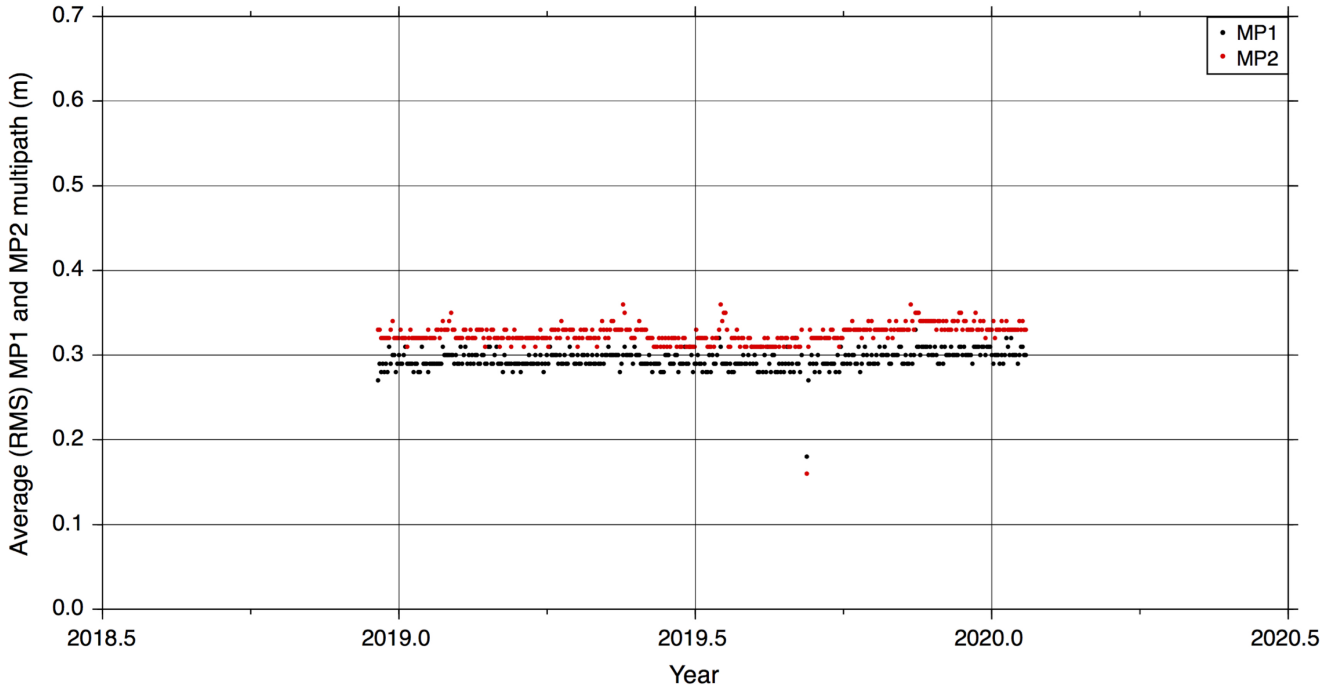

Figure S5. MP1 (black) and MP2 (red) values obtained from the analysis of the CAVO station data RINEX with TEQC software.

1 CORRELATIONS BETWEEN INDUSTRIAL ACTIVITY AND SEISMICITY

This method has been recently used for performing a large-scale screening to measure significant changes in background seismicity rates at the national scale in Italy (Garcia et al., 2021). The binomial test assumes independence between event occurrences, hence we first verify it on the inter-event times (IETs, defined as times between successive events) of the complete part of the catalog (as proposed in Bebbington, 2012). The results are shown as Figures S6 and S7, and support independence between the 10 seismic events, thus allowing us to reject a correlation between the duration of successive IETs. Let's call t_c the time at which a change (i.e., stop or re-start) in the industrial activity takes place; let $T_{pre} = [t_1, t_c]$ be the time interval identified before the stop (re-start) of the activity, and $T_{post} = [t_c, t_2]$ the time interval identified after the industrial activity stop (re-start). Let n_{pre} be the number of events that occurred in the period T_{pre}, and n_{post} the number of events that occurred in the period T_{post}. The total number of events in both periods is therefore $N = n_{pre} + n_{post}$. If the seismicity rate exhibit changes that are correlated with changes in the production trend before and after the time at which a change has occurred (t_c), that is, if the seismicity rate during T_{pre} is significantly different from the seismicity rate during T_{post}, then the actual division of the total number of events N in both periods into n_{pre} and n_{post} should be significantly different from the division which could be attained at random. Therefore, if we hypothesise stationary seismicity, the proposed null hypothesis, H_0, states that (for more details see Leptokaropoulos et al., 2017; Garcia et al., 2021):

$H_0 : n_{post}$ can be obtained at random from N under probability P

where P is related to the time partitions as follows:

$$P = \frac{T_{post}}{T_{pre} + T_{post}} \tag{S1}$$

This hypothesis is tested by means of the binomial test (e.g., Wonnacott and Wonnacott, 1977). If N events occur randomly in the whole interval $[t_1, t_2]$, this test provides (i) the probability p_1 that the number of events in the interval $[t_c, t_2]$ is less than or equal to n_{post},

$$p_1 = Pr\{n \leq n_{\text{post}}|N, P\} = \sum_{n=0}^{n_{\text{post}}} \binom{N}{n} P^n (1-P)^{N-n} \tag{S2}$$

or (ii) the probability p_2 that the number of events in the interval $[t_c, t_2]$ is greater than or equal to n_{post},

$$p_2 = Pr\{n \geq n_{\text{post}}|N, P\} = 1 - \sum_{n=0}^{n_{\text{post}}-1} \binom{N}{n} P^n (1-P)^{N-n} \tag{S3}$$

The binomial test assumes that each event is independent, with equal probability of occurrence in the interval $[t_1, t_2]$; H_0 is evaluated at a given significance level (e.g, $s.l. = 0.05$), so that if p_1 (or p_2) $< s.l.$, we conclude that there is evidence, with significance of $s.l.$, that the seismicity rate in the interval $[t_c, t_2]$ decreased (or increased) with respect to the $[t_1, t_c]$ seismicity rate.

This statistical test looks for potential significant seismicity rate changes correlated with the stop and re-start of the Cavone oil field's production activities. With this aim, in the experimentation period we identify three time intervals of interest ($T1$, $T2$, and $T3$ as in Figure 12), which correspond to the periods

preceding, during, and after the shutdown of industrial activities, respectively. The duration and number of events identified in these three time intervals are summarised in Table S5. If changes in seismicity rates are influenced by such changes in industrial operations, then we would expect that the rate of events in T2 exhibit some difference with respect to the rates observed in T1 or T3. We evaluated the possibility of observing after a given change point in industrial activity (i.e., stop or start) a number of events that is significantly lesser (Eq. S2) or greater (Eq. S3) than in the previous time interval. The results of this test are summarised in Table S6: in no case the p-values are small enough to reject the null hypothesis.

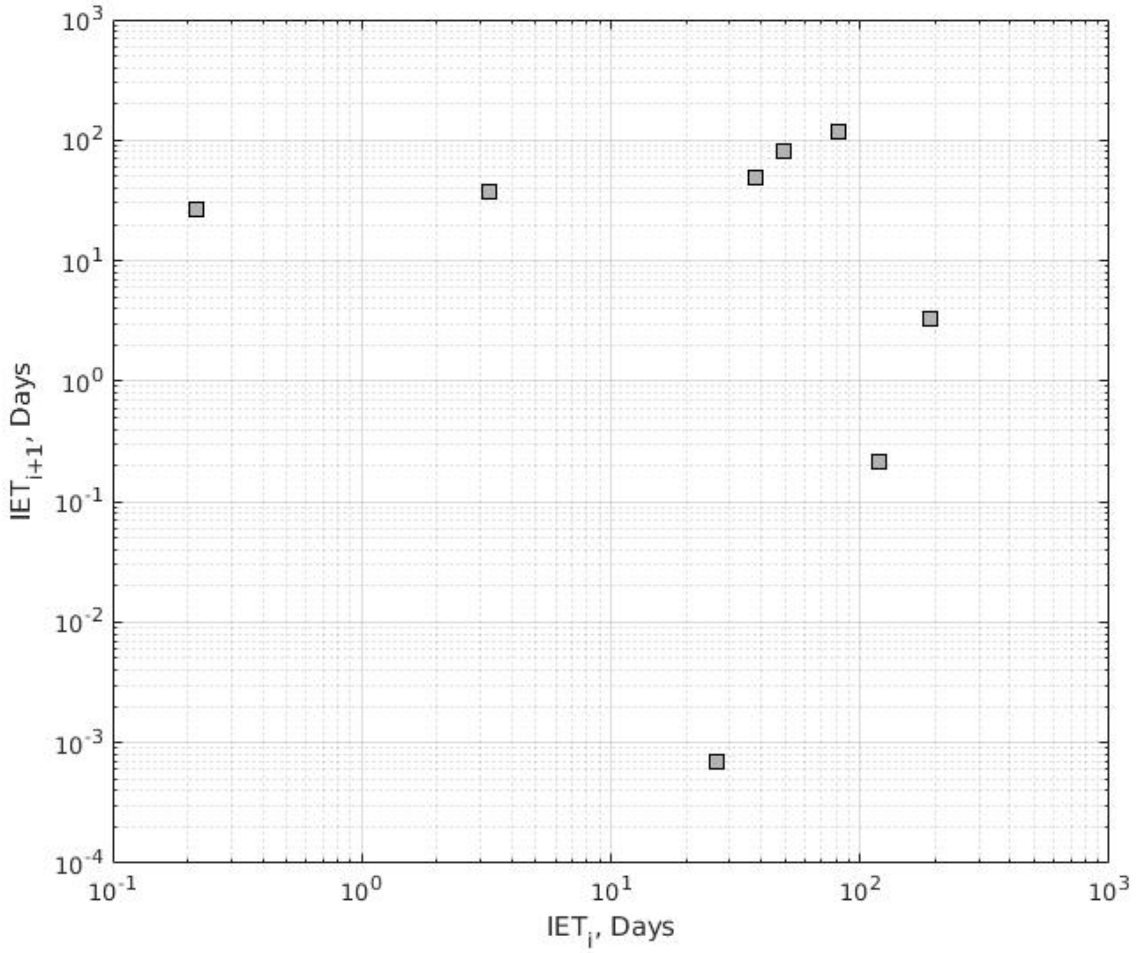

Figure S6. Plot of each IET versus the successive one, if there were a relationship it should be visible as a trend. We compute the Pearson (r^2) and the Spearman (ρ) coefficients testing for linear and not linear relationships, and obtaining $r^2 = -0.2$, with a p-value $= 0.6$, and $\rho \sim 0$, with a p-value ~ 1, thus rejecting any possible relationship between successive IET.

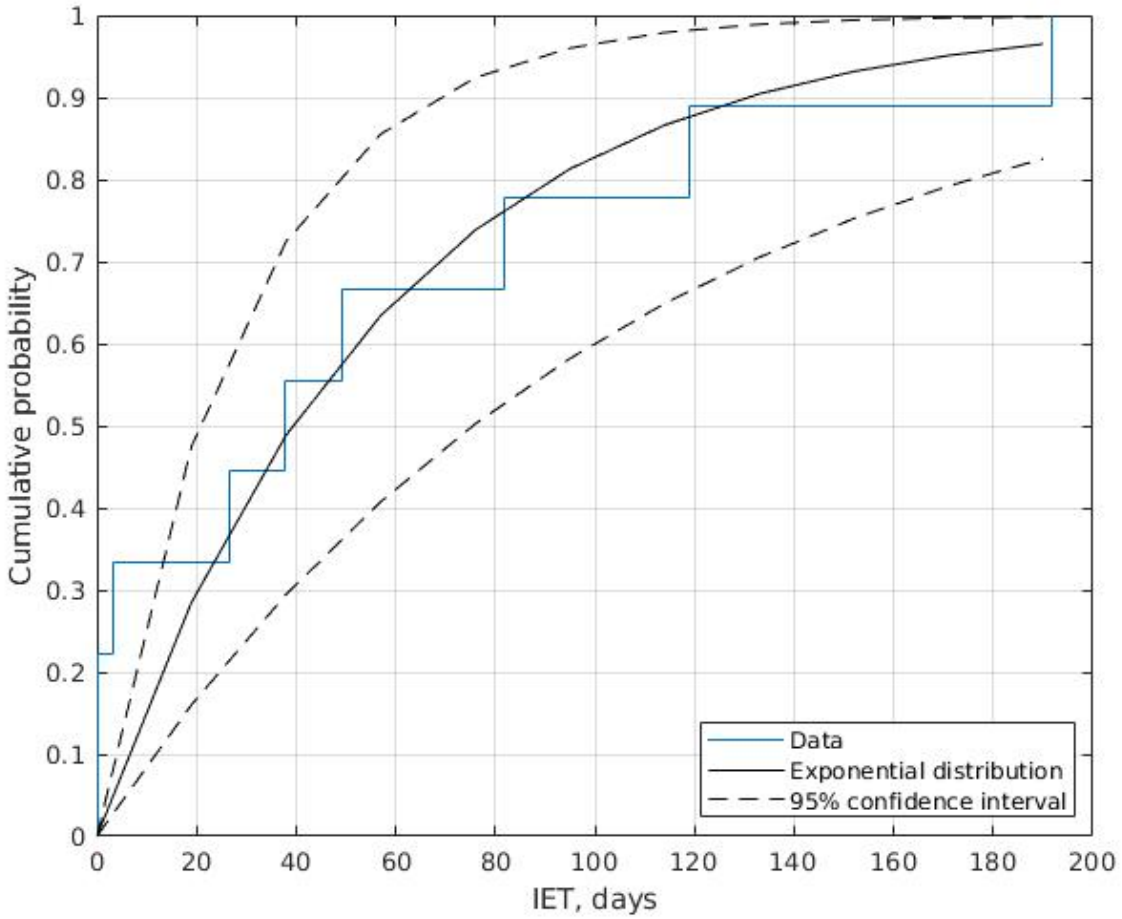

Figure S7. Plot of the cumulative distribution of the IET with comparison with the exponential probability distribution and its 95% confidence interval. The fact that our data fall inside this interval and that their $CV = 1.1$, ensure us about the possible exponential distribution of IET, thus confirming the seismic event independence.

Time Interval	**Start (day)**	**End (day)**	**Duration (days)**	Number of Events
T1	1	196	196	1
T2	197	320	124	3
T3	321	730	410	6

Table S5. Partition of the temporal intervals of interest in the monitoring period based on the industrial activity different stages. **T2** period identifies the shutdown period.

Test between...	p_1 **(Eq. S2) (lesser rate)**	p_2 **(Eq. S3) (greater rate)**
T1 - T2	0.98	0.17
T3 - T2	0.33	0.88

Table S6. Results of the binomial test considering changes in industrial activity between **T1** and **T2**, and between **T3** and **T2**.

REFERENCES

Bebbington, M. S. (2012). Models for temporal volcanic hazard. *Statistics in Volcanology* 1, 1–24

Garcia, A., Faenza, L., Morelli, A., and Antoncecchi, I. (2021). Can hydrocarbon extraction from the crust enhance or inhibit seismicity in tectonically active regions? a statistical study in italy. *Frontiers in Earth Science* 9, 497. doi:10.3389/feart.2021.673124

Govoni, A., Marchetti, A., and De Gori, P. (2014). The 2012 Emilia seismic sequence (Northern Italy): Imaging the thrust fault system by accurate aftershock location. *Tectonophysics* 622, 44–55. doi:10.1016/j.tecto.2014.02.013

Leptokaropoulos, K., Staszek, M., Lasocki, S., Martínez-Garzón, P., and Kwiatek, G. (2017). Evolution of seismicity in relation to fluid injection in the North-Western part of The Geysers geothermal field. *Geophysical Journal International* 212, 1157–1166. doi:10.1093/gji/ggx481

Marzocchi, W., Sandri, L., Heuret, A., and Funiciello, F. (2016). Where giant earthquakes may come. *J. Geophys. Res. Solid Earth* 121. doi:10.1002/2016JB013054

Peterson, J. (1993). Observation and modeling of seismic background noise. *U.S. Geol. Surv. Open-File Rept* 93, 94

Wiemer, S. and Wyss, M. (2000). Minimum magnitude of completeness in earthquake catalogs: Examples from Alaska, the western United States and Japan. *Bull. Seismol. Soc. Am.* 90(4), 859–869

Woessner, J. and Wiemer, S. (2005). Assessing the Quality of Earthquake Catalogs: Estimating the Magnitude of Completeness and Its Uncertainty. *Bull. Seismol. Soc. Am.* 95, 684–698

Wonnacott, T. and Wonnacott, R. J. (1977). *Introductory Statistics* (Wiley)